Solid State Sciences 146 (2023) 107373

Contents lists available at ScienceDirect

Solid State Sciences

journal homepage: www.elsevier.com/locate/ssscie

High-pressure/high-temperature synthesis of the new boron-rich terbium hydroxyborate $Tb_3B_{12}O_{19}(OH)_7$

Tobias A. Teichtmeister [a], Lkhamsuren Bayarjargal [b], Gunter Heymann [a], Hubert Huppertz [a,*]

[a] Department of General, Inorganic and Theoretical Chemistry, University of Innsbruck, Innrain 80–82, 6020, Innsbruck, Austria
[b] Institut für Geowissenschaften, Abt. Kristallographie/Mineralogie, Goethe-Universität, Altenhöferallee 1, D-60438, Frankfurt am Main, Germany

ARTICLE INFO

Keywords:
Borate
Crystal structure
High-pressure
Solid-state chemistry
Terbium

ABSTRACT

Monoclinic $Tb_3B_{12}O_{19}(OH)_7$ was obtained by multianvil high-pressure/high-temperature syntheses at 6 GPa and 650 °C. The crystal structure was investigated by single-crystal X-ray diffraction methods and space group *C*2 (no. 5) with the unit cell parameters $a = 24.2299(5)$ Å, $b = 4.4667(1)$ Å, $c = 7.0964(2)$ Å, $\beta = 94.58(1)°$, and two formula units per cell were revealed. Powder X-ray diffraction, infrared spectroscopy and the investigation of its second harmonic generation properties support the proposed structural model.

1. Introduction

Crystalline borates are known for their ability to form a plethora of various crystal structures, by the connection of linear [BO_2], trigonal planar [BO_3], and tetrahedral [BO_4] groups via common corners or edges. This and their wide optical transparency window combined with their chemical stability make them appealing materials for use in modern lighting technologies, non-linear optical applications, as well as laser and birefringent materials [1,2]. Lanthanoid borates in general and terbium borates especially already display a large variety of known crystal structures depending on the synthetic conditions. Under ambient pressure conditions, terbium plays the role of a transition point in the series of lanthanoid meta borates, in which the earlier elements form the α-*Ln*$(BO_2)_3$ (*Ln* = La–Nd, Sm–Tb) structure type [3–11], crystallizing in the monoclinic space group *I*2/*a* (no. 15), while smaller lanthanoids form the orthorhombic β-*Ln*$(BO_2)_3$ (*Ln* = Tb, Dy) structure [12–14] in the space group *Pnma* (no. 62). However, terbium can not only be found in both structure types depending on the ratio of terbium to boron during the synthesis [8], but the monoclinic phase α-$Tb(BO_3)_2$ also displays polymorphic behavior at low temperatures, where it undergoes a phase transition to space group $P2_1/c$ (no. 14) [15]. Additionally, the β-structural variant was found for Nd–Lu at elevated pressures [13,16, 17]. Outside the series of ortho- and meta-borates, several terbium borates were characterized. These include the high-pressure phase α-$Tb_2B_4O_9$ [18], featuring the rare structural motif of edge-sharing [BO_4] tetrahedra and the hydroxyl-containing borate $TbB_6O_9(OH)_3$ [19], which was synthesized in a flux of boric acid using steel autoclaves. Recently, we have also reported on another hydroxyl-containing terbium borate $Tb_3B_{10}O_{17}(OH)_5$ which was synthesized at 650 °C and 11 GPa in a multianvil high-pressure device [20]. In related experiments, we found that a certain pressure threshold is needed for the reaction to yield $Tb_3B_{10}O_{17}(OH)_5$, while a different crystal structure is formed at lower pressures. The product of these experiments, $Tb_3B_{12}O_{19}(OH)_7$, will be discussed in this article. Next to the determination of its crystal structure based on single-crystal X-ray diffraction, an infrared spectroscopic investigation and the second harmonic generation properties of the new compound will be presented.

2. Experimental section

2.1. High-pressure/high-temperature synthesis

High-pressure/high-temperature syntheses of $Tb_3B_{12}O_{19}(OH)_7$ were carried out in a modified Walker-type multianvil device (Max Voggenreiter GmbH, Mainleus, Germany), on which detailed information is available in the literature [21–23]. The starting materials Tb_4O_7 and H_3BO_3 were carefully weighed, intimately ground, and placed in an 18/11 assembly using a platinum capsule. Within 180 min, the sample was compressed to 6 GPa, subsequently heated to 650 °C in 10 min, and then the temperature was kept constant for the following 75 min. After quenching the reaction, the sample was decompressed within 540 min to ambient conditions and further isolated from the platinum capsule.

* Corresponding author. Department of General, Inorganic and Theoretical Chemistry, University of Innsbruck, Innrain 80–82, 6020, Innsbruck, Austria.
E-mail address: Hubert.Huppertz@uibk.ac.at (H. Huppertz).

https://doi.org/10.1016/j.solidstatesciences.2023.107373
Received 13 October 2023; Received in revised form 12 November 2023; Accepted 12 November 2023
Available online 16 November 2023

2.2. X-ray diffraction structure determination

Single-crystals of the new compounds were isolated under a polarization microscope. Measurements were carried out on a Bruker D8 Quest equipped with a Photon III C14 area detector. The programs SAINT (V8.40B) [24] and APEX4 (v2021.4.0) [25] were used for data collection and processing. A multi-scan absorption correction was carried out using the program SADABS (2016/2) [26,27], and the structure was solved via SHELXT (2018/2) [28,29] algorithms. According to the systematic extinctions, the possible space groups were *C*2/*m* (no. 12), *C*2 (no. 5), and *Cm* (no. 8). Space group *C*2 (no. 5) was finally derived since structure solution was only possible under these symmetry conditions. Structure refinements were calculated using SHELXL [30] algorithms incorporated into the program OLEX2 (Version 1.5) [31]. During the refinement of the crystal structure, seven reflections were omitted from the refinement due to their high deviation. O–H-distances within the crystal structure solutions were fixed at 0.83(2) Å. Symmetry checks of the final structures were performed employing the program package PLATON [32–36]. All atoms, excluding hydrogen, were refined anisotropically, and the structure and refinement data are shown in Tables 1–5..

Further details of the crystal structure investigation may be obtained from Fachinformationszentrum Karlsruhe, 76344 Eggenstein-Leopoldshafen, Germany (fax: +49-7247-808-666; e-mail: crysdata@fiz-karlsruhe.de, http://www.fiz-informationsdienste.de/en/DB/icsd/depot_anforderung.html) on quoting the deposition number CSD-2299368.

Table 1
Structural and refinement data for $Tb_3B_{12}O_{19}(OH)_7$.

Empirical formula	$Tb_3B_{12}O_{19}(OH)_7$
Molar mass, g•mol^{-1}	1029.54
Crystal system	monoclinic
Space group	*C*2 (no. 5)
Single-crystal data	
a, Å	24.2299(5)
b, Å	4.4667(1)
c, Å	7.0964(2)
β, deg	94.581(1)
Cell volume, Å^3	765.57(3)
Formula units per cell	2
Calculated density, g·cm^{-3}	4.466
Temperature, K	302(1)
Diffractometer	Bruker D8 Quest Photon III C14
Radiation type; wavelength, pm	Mo-K_α, 71.073
Absorption coefficient, mm^{-1}	13.879
F(000), e	940
Crystal size, mm^3	0.07 × 0.03 × 0.02
Range in *θ*, deg	3.219–42.142
Range in *hkl*	$h = \pm45$, $k = \pm8$, $l = \pm13$
Reflections collected	42772
Independent reflections	5391
Reflections with I ≥ 2σ(I)	5364
R_{int}/R_σ	0.0294/0.0166
Completeness to $\theta = 25.24°$, %	99.1
Refinement method	least squares on F^2
Data/restraints/parameters	5391/4/203
Flack parameter	−0.018(4)
Absorption correction	multi-scan
Final R1/w*R*2 [I ≥ 2σ(I)]	0.0108/0.0252
Final R1/w*R*2 (all data)	0.0109/0.0252
Goodness-of-Fit on F^2	1.054
Largest diff. peak/hole, e·Å^{-3}	0.964/-0.908
Powder diffraction data	
Diffractometer	STOE Stadi P
Radiation; *λ*, pm	Mo-$K_{\alpha1}$; 70.93
a, Å	24.3203(4)
b, Å	4.48408(7)
c, Å	7.1239(2)
β, deg	94.568(2)
Cell volume *V*, Å^3	774.42(3)
2*θ* Range, deg	2.000–40.385
2*θ* Step width, deg	0.015
R_{exp}	0.0107
R_{wp}	0.0672
R_p	0.0506

Table 2
Atom labels and corresponding Wyckoff-positions, atomic coordinates, and equivalent isotropic displacement parameters (U_{eq}) or isotropic displacement parameters (U_{iso}) for all crystallographically different atoms. U_{eq} is defined as one third of the trace of the orthogonalized U_{ij} tensor (standard deviations in parentheses).

Atom	Wyckoff-position	*x*	*y*	*z*	*S.O.F*	U_{eq}/U_{iso}*
Tb1	4*c*	0.18085(2)	0.13491(2)	0.16807(2)	1	0.00543(2)
Tb2	2*a*	0	0.00003(2)	0	1	0.00469(2)
B1	4*c*	0.06386(7)	0.4890(5)	0.3139(2)	1	0.0054(2)
B2	4*c*	0.13557(7)	0.2649(5)	0.5445(2)	1	0.0049(2)
B3	4*c*	0.27673(7)	0.6001(4)	0.2872(3)	1	0.0049(2)
B4	4*c*	0.31891(7)	0.0904(4)	0.1801(3)	1	0.0049(2)
B5	4*c*	0.40680(8)	0.0871(4)	0.0170(3)	1	0.0051(2)
B6	4*c*	0.41276(7)	0.2644(4)	0.3542(2)	1	0.0050(2)
O1	4*c*	0.51786(5)	0.7728(4)	0.2740(2)	1	0.0091(2)
O2	4*c*	0.09986(5)	0.0781(3)	0.6460(2)	1	0.0060(2)
O3	4*c*	0.11554(5)	0.3277(3)	0.3509(2)	1	0.0056(2)
O4	4*c*	0.19112(5)	0.1511(3)	0.5342(2)	1	0.0059(2)
O5	4*c*	0.27392(5)	0.2859(3)	0.2238(2)	1	0.0059(2)
O6	4*c*	0.28290(5)	0.1769(3)	0.6911(2)	1	0.0069(2)
O7	4*c*	0.29635(5)	0.7905(3)	0.1367(2)	1	0.0056(2)
O8	4*c*	0.34812(5)	0.1924(3)	0.0173(2)	1	0.0059(2)
O9	4*c*	0.36125(5)	0.0666(3)	0.3501(2)	1	0.0041(2)
O10	4*c*	0.40734(5)	0.7555(3)	0.0200(2)	1	0.0060(2)
O11	4*c*	0.44038(5)	0.2097(3)	0.1800(2)	1	0.0050(2)
O12	4*c*	0.44948(5)	0.1671(3)	0.5182(2)	1	0.0054(2)
O13	4*c*	0.56815(6)	0.1887(3)	0.1515(2)	1	0.0071(2)
H6	4*c*	0.286(2)	0.17(2)	0.582(5)	1	0.019(9)*
H10	4*c*	0.401(2)	0.68(2)	0.120(4)	1	0.03(2)*
H12	4*c*	0.483(2)	0.16(2)	0.49(2)	0.5	0.01(2)*
H1	4*c*	0.487(2)	0.84(2)	0.290(8)	1	0.07(2)*

Table 3
Anisotropic displacement parameters for all crystallographically different atoms.

Atom	U_{11}	U_{22}	U_{33}	U_{23}	U_{13}	U_{12}
Tb1	0.00482(3)	0.00607(3)	0.00544(3)	−0.00015(2)	0.00061(2)	0.00035(2)
Tb2	0.00452(4)	0.00498(4)	0.00453(4)	0	0.00019(3)	0
B1	0.0054(5)	0.0058(6)	0.0052(5)	0.0002(5)	0.0008(4)	0.0003(5)
B2	0.0049(5)	0.0050(6)	0.0048(5)	0.0002(5)	0.0006(4)	0.0002(5)
B3	0.0051(5)	0.0041(6)	0.0056(6)	0.0001(5)	0.0003(4)	−0.0003(4)
B4	0.0052(6)	0.0049(6)	0.0047(6)	0.0002(4)	0.0007(4)	−0.0001(4)
B5	0.0054(6)	0.0055(6)	0.0045(6)	−0.0003(4)	0.0004(4)	−0.0008(4)
B6	0.0053(5)	0.0045(5)	0.0053(5)	0.0000(5)	0.0010(4)	0.0002(5)
O1	0.0066(4)	0.0105(5)	0.0103(5)	−0.0045(4)	0.0015(4)	−0.0019(4)
O2	0.0082(4)	0.0041(4)	0.0058(4)	0.0001(3)	0.0024(3)	−0.0013(3)
O3	0.0057(4)	0.0079(5)	0.0032(4)	0.0006(3)	0.0003(3)	0.0022(3)
O4	0.0054(4)	0.0076(4)	0.0046(4)	−0.0001(4)	0.0003(3)	0.0024(4)
O5	0.0047(4)	0.0045(4)	0.0084(4)	−0.0015(4)	0.0006(3)	0.0003(3)
O6	0.0055(4)	0.0083(5)	0.0070(4)	−0.0002(3)	0.0014(3)	−0.0016(3)
O7	0.0075(4)	0.0045(4)	0.0047(4)	−0.0005(3)	0.0010(3)	−0.0015(4)
O8	0.0049(4)	0.0070(4)	0.0057(4)	0.0019(3)	0.0009(3)	0.0001(3)
O9	0.0033(4)	0.0052(4)	0.0037(4)	0.0019(3)	−0.0004(3)	−0.0009(3)
O10	0.0079(4)	0.0046(4)	0.0055(4)	0.0000(4)	0.0011(3)	−0.0002(4)
O11	0.0052(4)	0.0063(4)	0.0037(4)	−0.0013(3)	0.0009(3)	−0.0006(3)
O12	0.0043(4)	0.0073(5)	0.0044(4)	0.0018(3)	−0.0006(3)	−0.0004(3)
O13	0.0100(5)	0.0074(5)	0.0042(4)	0.0014(3)	0.0026(3)	0.0037(3)

X-ray powder diffraction patterns (Fig. 1) were collected on a STOE Stadi P powder diffractometer (STOE & CIE GmbH, Darmstadt, Germany) [37], equipped with a Ge(111) monochromator and a MYTHEN 1K detector system (Dectris Ltd., Baden Daettwil, Switzerland) [38]. The measurements were carried out overnight in Debye-Scherrer mode using a glass capillary with a diameter of 0.3 mm (Hilgenberg, Malsfeld, Germany) [39]. Using the Rietveld-method [40,41], a composition of 99 % of the title compound $Tb_3B_{12}O_{19}(OH)_7$ and 1 % of the low-temperature polymorph *LT*-$Tb(BO_2)_3$ (monoclinic; space group

Table 4
Selected interatomic distances (Å) and bond angles (deg) (standard deviations in parentheses) in $Tb_3B_{12}O_{19}(OH)_7$.

Atoms	Distance	Atoms	Distance
Tb1–O3	2.293(2)	Tb2–O1[e]	2.306(2)
Tb1–O5	2.357(2)	Tb2–O1[a]	2.306(2)
Tb1–O7[a]	2.378(2)	Tb2–O13[a]	2.353(2)
Tb1–O6[b]	2.411(2)	Tb2–O13[e]	2.353(2)
Tb1–O8[a]	2.446(2)	Tb2–O11[e]	2.386(2)
Tb1–O10[a]	2.486(2)	Tb2–O11[a]	2.386(2)
Tb1–O4	2.591(2)	Tb2–O10[a]	2.532(2)
Tb1–O6[c]	2.737(2)	Tb2–O10[e]	2.532(2)
Tb1–O8[d]	2.877(2)		
Average	2.502	Average	2.394
B1–O3	1.450(3)	B2–O2	1.437(3)
B1–O13[f]	1.467(3)	B2–O4	1.446(3)
B1–O1[e]	1.485(3)	B2–O3	1.447(3)
B1–O12[c]	1.490(3)	B2–O9[c]	1.541(3)
Average	1.473	Average	1.468
B3–O4[c]	1.452(3)	B4–O5	1.450(3)
B3–O7	1.474(3)	B4–O7[g]	1.470(3)
B3–O5	1.474(3)	B4–O8	1.474(3)
B3–O6[c]	1.505(3)	B4–O9	1.524(3)
Average	1.476	Average	1.480
B5–O13[h]	1.456(3)	B6–O2[c]	1.434(3)
B5–O11	1.466(3)	B6–O11	1.473(3)
B5–O10[g]	1.481(3)	B6–O12	1.473(3)
B5–O8	1.498(3)	B6–O9	1.527(3)
Average	1.475	Average	1.477
Atoms	Angle	Atoms	Angle
O3–B1–O13[f]	109.3(2)	O2–B2–O4	114.9(2)
O3–B1–O1[e]	109.6(2)	O2–B2–O3	114.8(2)
O3–B1–O12[c]	111.08(2)	O2–B2–O9[c]	105.9(2)
O13[f]–B1–O1[e]	110.2(2)	O4–B2–O3	105.3(2)
O13[f]–B1–O12[c]	109.7(2)	O4–B2–O9[c]	105.8(2)
O1[e]–B1–O12[c]	107.0(2)	O3–B2–O9[c]	106.9(2)
Average	109.5	Average	108.9
O4[c]–B3–O7	111.1(2)	O5–B4–O7[g]	108.7(2)
O4[c]–B3–O5	115.1(2)	O5–B4–O8	113.4(2)
O4[c]–B3–O6[c]	109.1(2)	O5–B4–O9	110.1(2)
O7–B3–O5	109.8(2)	O7[g]–B4–O8	108.1(2)
O7–B3–O6[c]	108.1(2)	O7[g]–B4–O9	108.5(2)
O5–B3–O6[c]	103.1(2)	O8–B4–O9	107.9(2)
Average	109.4	Average	109.5
O13[h]–B5–O11	106.9(2)	O2[c]–B6–O11	105.8(2)
O13[h]–B5–O10[g]	108.6(2)	O2[c]–B6–O12	113.9(2)
O13[h]–B5–O8	111.2(2)	O2[c]–B6–O9	113.0(2)
O11–B5–O10[g]	111.0(2)	O11–B6–O12	109.1(2)
O11–B5–O8	110.4(2)	O11–B6–O9	108.3(2)
O10[g]–B5–O8	108.7(2)	O12–B6–O9	106.6(2)
Average	109.5	Average	109.5

Symmetry operators for generating equivalent atoms:

[a] -*x*+1/2, *y*-1/2, -*z*
[b] -*x*+1/2, *y*-1/2, -*z*+1
[c] -*x*+1/2, *y*+1/2, -*z*+1
[d] -*x*+1/2, *y*+1/2, -*z*
[e] *x*-1/2, *y*-1/2, *z*
[f] *x*-1/2, *y*+1/2, *z*
[g] *x*, *y*-1, *z*
[h] -*x*+1, *y*, -*z*

Table 5
Hydrogen bond parameters in $Tb_3B_{12}O_{19}(OH)_7$.

Atoms	D–H/Å	H···A/Å	D–H···A/Å	D–H···A/deg
O1–H1···O11	0.82(3)	2.13(6)	2.753(3)	133
O10–H10···O2	0.82(2)	1.72(4)	2.518(2)	165
O12–H12···O12	0.84(3)	1.65(4)	2.483(2)	168

$P2_1/c$, no. 14) [15] was found in the powder sample. Noticeably, the residual intensity of one reflection at 10.9° could not be reliably assigned to a known side-phase.

2.3. Infrared spectroscopy

A Bruker Alpha Platinum attenuated total reflection (ATR) spectrometer was used to collect infrared spectra of $Tb_3B_{12}O_{19}(OH)_7$. Measurements were carried out on the bulk material and the spectra were measured in the range of 4000 to 400 cm^{-1}. The data was processed and corrected for atmospheric influences employing the OPUS 7.2 [42] software.

2.4. Second harmonic generation measurements

Second harmonic generation (SHG) measurements were performed on a powder sample of $Tb_3B_{12}O_{19}(OH)_7$ using the Kurtz-Perry approach [43]. We used quartz, KDP (KH_2PO_4), and corundum (Al_2O_3) for reference measurements. A Q-switched Nd:YAG laser (1064 nm, 5–6 ns, 2 kHz) was used for the generation of the fundamental pump wave. The fundamental infrared light was separated using a harmonic separator, a short-pass filter, and an interference filter from the generated second harmonic (532 nm). The generated SHG signal was collected with a photomultiplier and an oscilloscope from six different areas of the sample. On each position, 64 pulses were measured and averaged. Background signals between the laser pulses were used to correct the measured intensities. The SHG measurements were performed under ambient conditions in transmission geometry.

3. Results and discussion

3.1. Crystal structure description

$Tb_3B_{12}O_{19}(OH)_7$ crystallizes monoclinically with the unit cell parameters $a = 24.2299(5)$ Å, $b = 4.4667(1)$ Å, $c = 7.0964(2)$ Å, $\beta = 94.58(1)°$, and two formula units per cell in space group $C2$ (no. 5). The composition $Tb_3B_{12}O_{19}(OH)_7$ equates to a Tb:B ratio of 1:4, which is the second highest among the existing terbium borates $TbB_6O_9(OH)_3$ (1:6), α-$Tb_2B_4O_9$ (1:2), $Tb_3B_{10}O_{17}(OH)_5$ (3:10), and the various forms of Tb $(BO_2)_3$ (1:3) and $TbBO_3$ (1:1) [8,12,15,18–20]. Two differently coordinated Tb-sites are found within the crystal structure. The Tb1 atom is nine-fold coordinated by oxygen with Tb–O-distances ranging from 2.293(2) to 2.877(2) Å, while the Tb2-site is coordinated by eight oxygen atoms in a square antiprismatic geometry with interatomic Tb–O-distances between 2.306(2) and 2.533(2) Å. These interatomic distances are well in the range of typical Tb–O-distances in borates [8, 12,15,18–20]. Due to the lower coordination number around the Tb2-site, lower interatomic distances are expected [44]. In Fig. 2, a graphical depiction of the two crystallographically different terbium-centered polyhedra is shown.

Six crystallographically different boron atoms build up a corrugated layered structure. All boron atoms are tetrahedrally coordinated by oxygen with interatomic distances within the tetrahedra varying between 1.434(3) and 1.541(3) Å. These interatomic distances fit well with the value of 1.48(4) Å [45], which is often cited as the standard value for bond lengths within $[BO_4]$ tetrahedra. Interatomic angles within the $[BO_4]$ tetrahedra only display a slight variance around the expected tetrahedral angle of 109.4(3)° [45]. The corrugated layers are formed from a repetitive building block, which is shown in Fig. 3. The O9 atom connects three $[BO_4]$ tetrahedra, namely those centered by the B2, B4, and B6 atoms. Several three-membered rings are formed within one building block, but also through the connection of two building blocks. Within one building block, the B1, B2, and B6, as well as the B2, B3, and B4 tetrahedra (e.g., a tetrahedron centered by the respective boron atom) form two three-membered rings. The B5 tetrahedron of one building block is connected to the B4 and B6 tetrahedra of an adjacent building block to form another three-membered ring. Furthermore, two building blocks are also connected via the formation of a four-membered ring, which consists of the B4 and B6 tetrahedra of one building block and the B2 and B3 tetrahedra of another. Finally, the connection of four

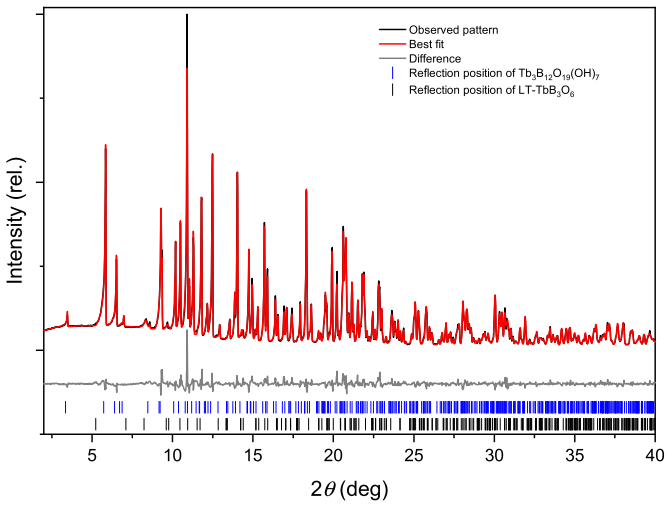

Fig. 1. Powder diffraction pattern (Mo-$K_{\alpha 1}$ - λ = 70.93 pm) and Rietveld-refinement of a binary mixture of 99 % $Tb_3B_{12}O_{19}(OH)_7$ and 1 % *LT*-$Tb(BO_2)_3$ [15].

building blocks yields nine-membered rings, which are built up by the B1, B5, and B6 tetrahedra of two building blocks, the B3 and B4 tetrahedra of the third building block, and the B4 tetrahedra of the fourth building block.

Along the crystallographic *a*-axis, an ABCD-stacking of these layers can be described. The Tb1 atoms are located in zigzag-channels between two adjacent layers. Thus, double-layers are formed, which are connected to the next double-layer via the Tb2-centered polyhedra. Each double-layer is turned 180° compared to the adjacent double-layer, yielding the final crystal structure depicted in Fig. 4.

The hydrogen positions were assigned after calculating the bond valence sums according to the bond-length/bond-strength (BLBS) [46] and the charge distribution (CHARDI) [47] concept. The results are shown in Table 6. The calculations indicate the expected oxidation state +III for the terbium atoms, hence seven hydrogen atoms are necessary for charge neutrality. Without the consideration of hydrogen in the calculation of the bond valence sums, large deviations from the expected value of −2 are found for the O1, O6, O10, and O12 atoms. Therefore, we conclude that the hydrogen atoms should be found on these positions. Looking at the symmetry of the crystal structure, it is apparent that the H12 atom can only be described by a half-occupied site (i.e., one hydrogen binding to the O12 while forming a hydrogen bond to another O12 atom). In total, this yields seven hydrogen atoms found on the four positions proposed from the calculation of the valence bond sums. If these hydrogen atoms are considered in the calculations, all values adjust closely to the expected values.

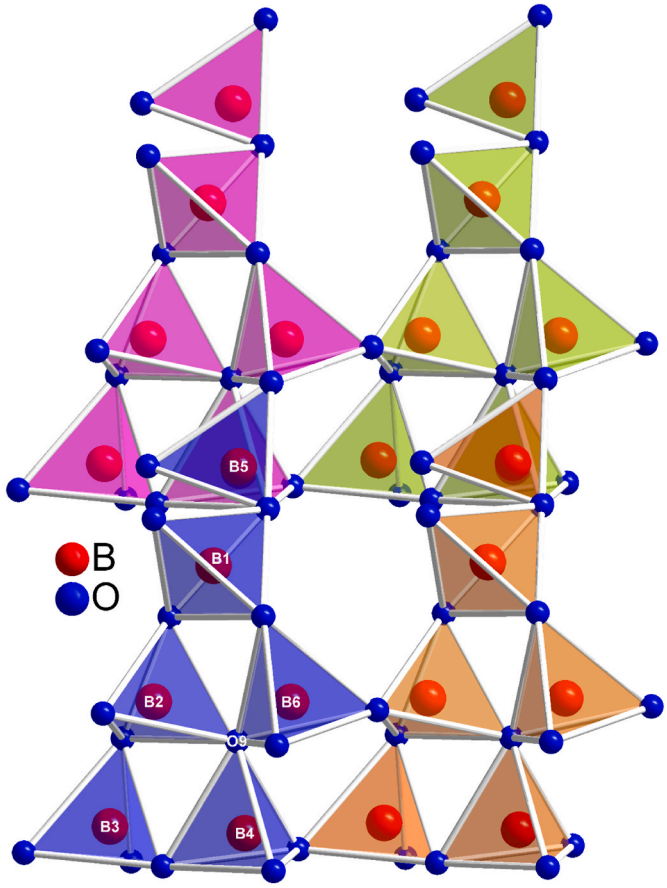

Fig. 3. Corrugated layers are formed in the *bc*-plane, built up by a repetitive $[B_6O_{13}]^{8-}$ building block. Each building block is shown in its own colour.

A plethora of hydrogen bonds, which play an important role in the connection of two adjacent layers, could be described in the crystal structure of $Tb_3B_{12}O_{19}(OH)_7$. Generally, interatomic donor−hydrogen···acceptor-distances up to 3.2 Å can be considered for hydrogen-bonding if the corresponding angle is larger than 90° [48]. However, due to the large number of possible hydrogen bonds in $Tb_3B_{12}O_{19}(OH)_7$, a focus on stronger hydrogen bonds with distances up to 3 Å and angles higher than 120° [48] seems advisable. These hydrogen bonds are listed in Table 5. Judging from the geometrical parameters, the strongest H-bond in $Tb_3B_{12}O_{19}(OH)_7$ is found for the H12 atom, which is located between two O12 atoms at a distance of 0.84 (3) Å from the donor and 1.65(4) Å from the acceptor atom with an angle of 168°. Also for the H10, a strong hydrogen bond is found with the O2

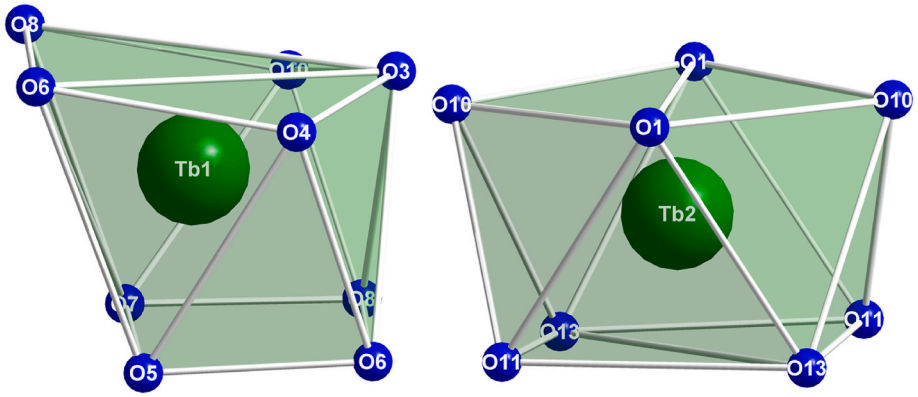

Fig. 2. Coordination environments of the two crystallographically different terbium atoms.

acting as an acceptor at a distance of 1.72(4) Å, while for the H1 and H6 atoms, only significantly weaker hydrogen bonds can be described. In the case of the atom H6, possible acceptor atoms are only found in the larger range for usual hydrogen bonds at distances between 3 and 3.2 Å. Since electron densities are detected by X-ray diffraction, it is noteworthy that hydrogen atoms are generally found too close to the respective oxygen site [48].

As a result of related experiments, we have recently presented the crystal structure of $Tb_3B_{10}O_{17}(OH)_5$, which was synthesized at similar temperatures but higher pressures of 11 GPa [20], while $TbB_6O_9(OH)_3$ was synthesized at lower pressures in a flux of boric acid [19]. A close comparison of the crystal structures of $TbB_6O_9(OH)_3$ and $Tb_3B_{10}O_{17}(OH)_5$ with the title compound $Tb_3B_{12}O_{19}(OH)_7$ reveals structural relationships typically observed in high-pressure crystal chemistry. $TbB_6O_9(OH)_3$ displays a crystal structure built up by trigonal $[BO_3]$ and tetrahedral $[BO_4]$ units [19], while, in agreement with the pressure coordination rule [44], boron is exclusively found tetrahedrally coordinated in $Tb_3B_{10}O_{17}(OH)_5$ [20] and the title compound $Tb_3B_{12}O_{19}(OH)_7$, which were synthesized at pressures of 11 and 6 GPa, respectively. Comparing the two high-pressure phases, an increase of the coordination number of the terbium atoms from C.N. 9 and 8 in $Tb_3B_{12}O_{19}(OH)_7$ to C.N. 10 and 11 for the atoms Tb1 and Tb2, respectively, in $Tb_3B_{10}O_{17}(OH)_5$ is also observed [20]. Furthermore, the increase in the coordination numbers aligns with the expected increase of Tb–O-distances [20,44].

3.2. Second harmonic generation measurements

$Tb_3B_{12}O_{19}(OH)_7$ displays a strong SHG-signal comparable to the intensity of KDP and around 6.3 times the corresponding signal of quartz. These results confirm that $Tb_3B_{12}O_{19}(OH)_7$ crystallizes non-centrosymmetrically [43], which is coherent with space group *C*2 (no. 5) derived from the single-crystal diffraction data. The measured SHG-intensities of $Tb_3B_{12}O_{19}(OH)_7$ and well-known reference materials are shown in Table 7. The strong SHG intensity of $Tb_3B_{12}O_{19}(OH)_7$ and a comparison with the weak SHG intensity of $Tb_3B_{10}O_{17}(OH)_5$ [20] indicate possible phase matching conditions like in KDP. Whether the title compound fulfills a phase matching condition can be determined by precise refractive measurements on large single crystals or by a correlation between SHG intensities and fine resolved grain sizes. However, such a determination was not performed in this work.

The crystal structure of $Tb_3B_{12}O_{19}(OH)_7$ is exclusively built up of $[BO_4]$ tetrahedra. Therefore, considering the weak SHG signals of comparable hydroxyborates like $Tb_3B_{10}O_{17}(OH)_5$ [20] and $La_3B_6O_{13}(OH)$ [49], the strong SHG effect observed in the title compound $Tb_3B_{12}O_{19}(OH)_7$ comes unexpected, since trigonal planar $[BO_3]$ groups are beneficial to a compound's nonlinear optical properties due to increased anisotropic effects [1,2]. This effect is further enhanced in fluor- and fluoroxoborates as precedented in the compounds $[CNH_2)_3][B_3O_3F_2(OH)_2]$, $[C[NH_2]_2]_2[B_3O_3F_4(OH)]$ and $C(NH_2)_3BF_4$ [50,51].

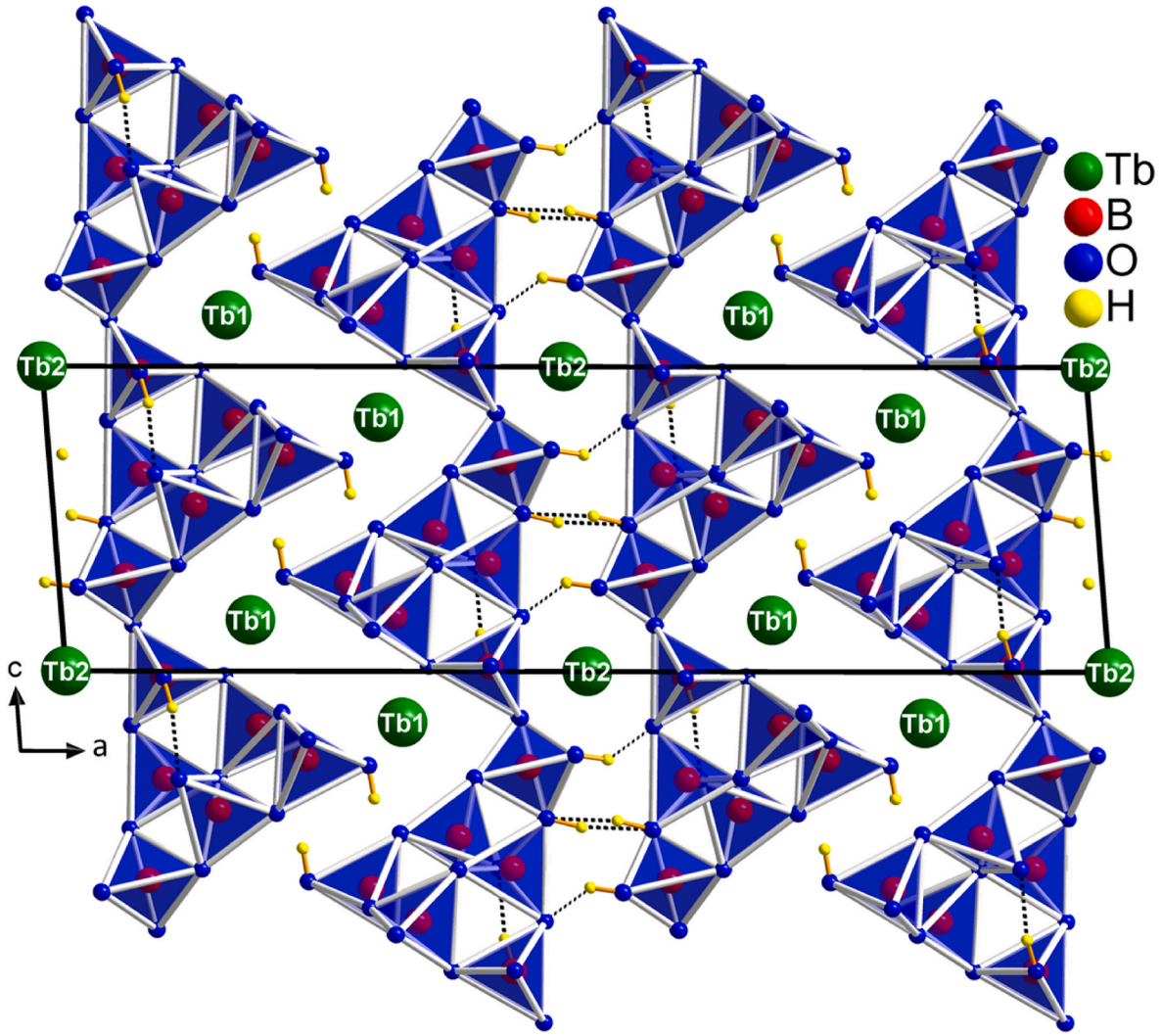

Fig. 4. The layered structure of $Tb_3B_{12}O_{19}(OH)_7$ is shown in its unit cell in the *ac*-plane.

Table 6
Calculation of bond valences with BLBS [46] (∑V) and CHARDI-2015 [47] (∑Q).

Atom	Without hydrogen		Hydrogen at O1, O6, O10, O12	
	∑V	∑Q	∑V	∑Q
Tb1	2.75	3.45	2.75	2.91
Tb2	3.08	3.11	3.08	2.92
B1	3.04	3.23	3.04	2.91
B2	3.10	3.20	3.10	3.13
B3	3.02	3.47	3.02	2.97
B4	2.99	3.12	2.99	3.12
B5	3.02	3.01	3.02	3.00
B6	3.01	3.40	3.01	3.19
O1	−1.21	−1.63	−2.14	−2.14
O2	−1.68	−1.73	−2.11	−1.86
O3	−2.10	−2.15	−2.10	−2.16
O4	−1.84	−1.89	−1.84	−1.88
O5	−1.98	−2.06	−1.98	−2.06
O6	−1.21	−1.21	−2.14	−2.21
O7	−1.92	−1.97	−1.92	−1.98
O8	−1.89	−1.89	−1.89	−1.89
O9	−1.95	−1.74	−1.95	−1.74
O10	−1.29	−1.56	−2.16	−2.18
O11	−1.92	−2.30	−1.92	−1.96
O12	−1.49	−1.47	−2.15	−1.96
O13	−1.98	−2.41	−1.98	−1.99

Table 7
Measured SHG-intensities of $Tb_3B_{12}O_{19}(OH)_7$, quartz, corundum, and KDP.

Samples	I_{SHG}/mV	I_{SHG}/I_{Quartz} *100 %
Quartz (5–25 μm)	77(23)	100
Al_2O_3 (9 μm)	0(1)	0
KDP (5–25 μm)	450(92)	584
$Tb_3B_{12}O_{19}(OH)_7$ (5–30μm)	487(66)	632

3.3. Infrared spectroscopy

In Fig. 5, the attenuated total reflection infrared spectrum of $Tb_3B_{12}O_{19}(OH)_7$ is presented. At wavenumbers between 3200 and 3500 cm^{-1}, a broad signal, that can be attributed to OH stretching vibrations, is observed [52,53]. Usually, signals between 1200 and 1500 cm^{-1} in borates are assigned to trigonal $[BO_3]$ groups or vibration modes involving three-fold coordinated oxygen atoms [54,55]. In $Tb_3B_{12}O_{19}(OH)_7$, only the latter are found. Hence, these signals are coherent with our structural model. At wavenumbers 800-1100 cm^{-1}, the stretching modes of $[BO_4]$ tetrahedra are observed, and at lower wavenumbers, bending modes of $[BO_4]$ tetrahedra and vibrations of the lanthanoid-centered polyhedra contribute increasingly to the observed signals [55,56].

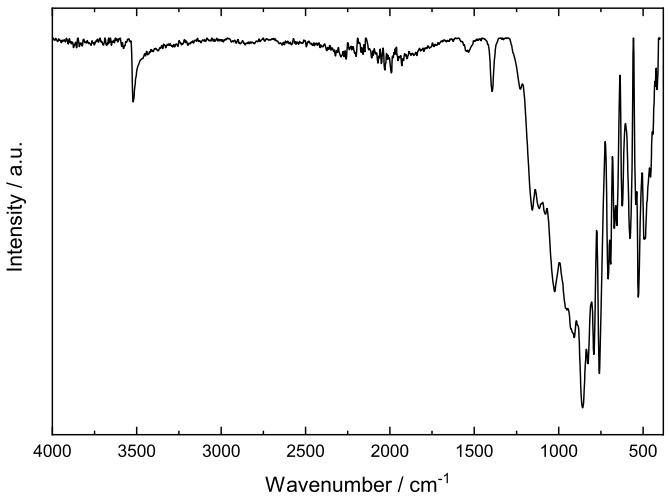

Fig. 5. The infrared spectrum of $Tb_3B_{12}O_{19}(OH)_7$.

4. Conclusion

The new hydroxyl-containing terbium borate $Tb_3B_{12}O_{19}(OH)_7$ was prepared by high-pressure/high-temperature syntheses using the multianvil technique. It displays a monoclinic layered crystal structure of corner-sharing $[BO_4]$ tetrahedra built up by a repetitive $[B_6O_{13}]^{8-}$ building block. An infrared spectroscopic investigation is coherent with the proposed structural model, and measurements of the non-linear optical properties of a powder sample yield a strong SHG effect comparable to KDP, thus confirming the non-centrosymmetric space group *C*2 (no. 5).

CRediT authorship contribution statement

Tobias A. Teichtmeister: Writing – original draft, Investigation, Visualization, Data curation. **Lkhamsuren Bayarjargal:** Investigation, Resources, Writing – review & editing. **Gunter Heymann:** Investigation, Writing – review & editing. **Hubert Huppertz:** Writing – review & editing, Resources.

Declaration of competing interest

The authors declare that they have no known competing financial interests or personal relationships that could have appeared to influence the work reported in this paper.

Data availability

Further details of the crystal structure investigation may be obtained from Fachinformationszentrum Karlsruhe on quoting the deposition number CSD-2299368.

Acknowledgement

The authors want to thank the Vice Rector for Research for the grant of a doctoral fellowship at the University of Innsbruck.

Appendix A. Supplementary data

Supplementary data to this article can be found online at https://doi.org/10.1016/j.solidstatesciences.2023.107373.

References

[1] M. Mutailipu, K.R. Poeppelmeier, S. Pan, Borates: a rich source for optical materials, Chem. Rev. 121 (2021) 1130–1202, https://doi.org/10.1021/acs.chemrev.0c00796.
[2] H. Huppertz, R. Ziegler, Borate applications, in: R. Pöttgen, T. Jüstel, C.A. Strassert (Eds.), Applied Inorganic Chemistry, Walter De Gruyter, Berlin/Boston, 2023, pp. 153–165. Ch. 6.3.
[3] J. St Ysker, W. Hoffmann, Die Kristallstruktur des $La[B_3O_6]$, Naturwissenschaften 57 (1970) 129, https://doi.org/10.1007/BF00600055.
[4] V.I. Pakhomov, G.B. Silnitskaya, A.V. Medvedev, B.F. Dzhurinskii, The crystal structure of neodymium metaborate, Izv. Akad. Nauk SSSR, Neorg. Mater. (1972) 1259–1263.
[5] G.K. Abdullaev, K. Mamedov, G.G. Dzhafarov, Crystal Structures of the Metaborates $Sm(BO_2)_3$ and $Gd(BO_2)_3$, Kristallografiya, 1975, pp. 265–269.
[6] G.K. Abdullaev, K. Mamedov, G.G. Dzhafarov, The refined crystal structure of lanthanum metaborate $La(BO_2)_3$, Kristallografiya (1981) 837–840.
[7] C. Sieke, T. Nikelski, T. Schleid, $Pr(BO_2)_3$ und $PrCl(BO_2)_2$: zwei meta-Borate des Praseodyms im Vergleich, Z. Anorg. Allg. Chem. 628 (2002) 819, https://doi.org/10.1002/1521-3749(200205)628:4<819:AID-ZAAC819>3.0.CO;2-E.
[8] A. Goriounova, P. Held, P. Becker, L. Bohatý, Monoclinic modification of polymorphic TbB_3O_6, Acta Crystallogr. E59 (2003) i83–i85, https://doi.org/10.1107/S1600536803009553.

[9] H. Müller-Bunz, T. Nikelski, T. Schleid, Einkristalle des Neodym(III)-*meta*-Borats $Nd(BO_2)_3$ und -*ortho*-Borats $Nd[BO_3]$, Z. Naturforsch. 58b (2003) 375–380, https://doi.org/10.1515/znb-2003-0503.

[10] A. Goriounova, P. Held, P. Becker, L. Bohatý, Cerium triborate, CeB_3O_6, Acta Crystallogr. E60 (2004) i134–i135, https://doi.org/10.1107/S1600536804024365.

[11] A. Goriounova, P. Held, P. Becker, L. Bohatý, Europium triborate, EuB_3O_6, Acta Crystallogr. E60 (2004) i131–i133, https://doi.org/10.1107/S1600536804024353.

[12] T. Nikelski, T. Schleid, Synthese und Kristallstruktur von Terbium(III)-*meta*-Oxoborat $Tb(BO_2)_3$ ($\equiv TbB_3O_6$), Z. Anorg. Allg. Chem. 629 (2003) 1017–1022, https://doi.org/10.1002/zaac.200200446.

[13] H. Emme, T. Nikelski, T. Schleid, R. Pöttgen, M.H. Möller, H. Huppertz, High-pressure synthesis, crystal structure, and properties of the new orthorhombic rare-earth *meta*-oxoborates $RE(BO_2)_3$ (RE = Dy–Lu), Z. Naturforsch. 59b (2004) 202–215, https://doi.org/10.1515/znb-2004-0213.

[14] T. Nikelski, M.C. Schäfer, H. Huppertz, T. Schleid, Crystal structure of dysprosium meta-oxoborate, β-$Dy(BO_2)_3$, via normal-pressure synthesis, Z. Kristallogr. N. Cryst. Struct. 223 (2008) 177–178, https://doi.org/10.1524/ncrs.2008.0073.

[15] P. Becker, R. Fröhlich, Polymorphy of monoclinic terbium triborate, TbB_3O_6, Cryst. Res. Technol. 43 (2008) 1240–1246, https://doi.org/10.1002/crat.200800397.

[16] H. Emme, G. Heymann, A. Haberer, H. Huppertz, High-pressure syntheses, crystal structures, and thermal behaviour of β-$RE(BO_2)_3$ (RE = Nd, Sm, Gd), Z. Naturforsch. 62b (2007) 765–770, https://doi.org/10.1515/znb-2007-0603.

[17] B. Fuchs, H. Huppertz, β-$Eu(BO_2)_3$ – a new member of the β-$RE(BO_2)_3$ (RE = Y, Nd, Sm, Gd–Lu) structure family, Z. Naturforsch. 74b (2019) 685–692, https://doi.org/10.1515/znb-2019-0117.

[18] H. Emme, H. Huppertz, High-pressure preparation, crystal structure, and properties of α-$(RE)_2B_4O_9$ (RE = Eu, Gd, Tb, Dy): oxoborates displaying a new type of structure with edge-sharing BO_4 tetrahedra, Chem. Eur J. 9 (2003) 3623–3633, https://doi.org/10.1002/chem.200204696.

[19] L. Li, P. Lu, Y. Wang, X. Jin, G. Li, Y. Wang, L. You, J. Lin, Synthesis of rare earth polyborates using molten boric acid as a flux, Chem. Mater. 14 (2002) 4963–4968, https://doi.org/10.1021/cm0203870.

[20] T.A. Teichtmeister, C. Paulsen, S.J. Ambach, K. Wurst, L. Bayarjargal, W. Schnick, H. Huppertz, High-pressure synthesis, crystal structure, and characterization of the new non-centrosymmetric terbium borate $Tb_3B_{10}O_{17}(OH)_5$, J. Solid State Chem. 325 (2023), 124170, https://doi.org/10.1016/j.jssc.2023.124170.

[21] D. Walker, Lubrication, gasketing, and precision in multianvil experiments, Am. Mineral. 76 (1991) 1092–1100.

[22] H. Huppertz, Multianvil high-pressure/high-temperature synthesis in solid state chemistry, Z. Kristallogr. 219 (2004) 330–338.

[23] D. Walker, M.A. Carpenter, C.M. Hitch, Some simplifications to multianvil devices for high pressure experiments, Am. Mineral. 75 (1990) 1020–1028.

[24] Bruker AXS Inc, SAINT, Bruker AXS Inc, Madison (WI), USA, 2021.

[25] Bruker AXS Inc, APEX4, Bruker AXS Inc, Madison (WI), USA, 2021.

[26] Bruker AXS GmBH, SADABS, Bruker AXS GmBH, Karlsruhe (Germany) (2016).

[27] L. Krause, R. Herbst-Irmer, G.M. Sheldrick, D. Stalke, Comparison of silver and molybdenum microfocus X-ray sources for single-crystal structure determination, J. Appl. Crystallogr. 48 (2015) 3–10, https://doi.org/10.1107/S1600576714022985.

[28] G.M. Sheldrick, Shelxt - integrated space group and crystal structure determination, Acta Crystallogr. A71 (2015) 3–8.

[29] Bruker AXS Inc, SHELXT - Crystal Structure Solution, Bruker AXS Inc, 2018.

[30] G.M. Sheldrick, Crystal structure refinement with SHELXL, Acta Crystallogr. C71 (2015) 3–8, https://doi.org/10.1107/S2053229614024218.

[31] O.V. Dolomanov, L.J. Bourhis, R.J. Gildea, J.A.K. Howard, H. Puschmann, OLEX2 a complete structure solution, refinement and analysis program, J. Appl. Crystallogr. 42 (2009) 339–341, https://doi.org/10.1107/S0021889808042726.

[32] A.L. Spek, Single-crystal structure validation with the program PLATON, J. Appl. Crystallogr. 36 (2003) 7–13, https://doi.org/10.1107/S0021889802022112.

[33] A.L. Spek, Structure validation in chemical crystallography, Acta Crystallogr. D65 (2009) 148–155, https://doi.org/10.1107/S090744490804362X.

[34] A.L. Spek, Platon squeeze: a tool for the calculation of the disordered solvent contribution to the calculated structure factors, Acta Crystallogr. C71 (2015) 9–18, https://doi.org/10.1107/S2053229614024929.

[35] A.L. Spek, What makes a crystal structure report valid? Inorg. Chim. Acta. 470 (2018) 232–237, https://doi.org/10.1016/j.ica.2017.04.036.

[36] A.L. Spek, checkCIF validation ALERTS: what they mean and how to respond, Acta Crystallogr. E76 (2020) 1–11, https://doi.org/10.1107/S2056989019016244.

[37] STOE & CIE GmbH, Stadi P, The Rapid Comprehensive Modular System with Unsurpassed Reliability, STOE & CIE GmbH, 2018.

[38] B.-D. Dectris Ltd, Technical Documentation: MYTHEN Detector System, B.-D. Dectris Ltd, 2015.

[39] STOE & CIE GmbH, Accessories, STOE & CIE GmbH (2018). Darmstadt (Germany).

[40] H.M. Rietveld, A profile refinement method for nuclear and magnetic structures, J. Appl. Crystallogr. 2 (1969) 65–71, https://doi.org/10.1107/S0021889869006558.

[41] D.K. Smith, J. Fiala, E. Ryba, Book reviews - the Rietveld method, Young R. A, Powder Diffr. 8 (1993) 252–254, https://doi.org/10.1017/S0885715600019497.

[42] Bruker Corporation, OPUS, Bruker Corporation, Billerica, MA, USA, 2012.

[43] S.K. Kurtz, T.T. Perry, A powder technique for the evaluation of nonlinear optical materials, J. Appl. Phys. 39 (1968) 3798–3813, https://doi.org/10.1063/1.1656857.

[44] C.T. Prewitt, R.T. Downs, High-pressure crystal chemistry, Rev. Mineral. Geochem. 37 (1998) 284–318.

[45] E. Zobetz, Geometrische Größen und einfache Modellrechnungen für BO_4 -Gruppen, Z. Kristallogr. 191 (1990) 45–57, https://doi.org/10.1524/zkri.1990.191.1-2.45.

[46] N.E. Brese, M. O'Keeffe, Bond-valence parameters for solids, Acta Crystallogr. B47 (1991) 192–197, https://doi.org/10.1107/S0108768190011041.

[47] M. Nespolo, B. Guillot, CHARDI2015 charge distribution analysis of non-molecular structures, J. Appl. Crystallogr. 49 (2016) 317–321, https://doi.org/10.1107/S1600576715024814.

[48] T. Steiner, The hydrogen bond in the solid state, Angew. Chem. Int. Ed. 41 (2002) 48–76, https://doi.org/10.1002/1521-3773(20020104)41:1<48:AID-ANIE48>3.0.CO;2-U.

[49] B. Fuchs, G. Heymann, X. Wang, A. Tudi, L. Bayarjargal, R. Siegel, A. Schmutzler, J. Senker, B. Joachim-Mrosko, A. Saxer, Z. Yang, S. Pan, H. Huppertz, $La_3B_6O_{13}(OH)$: the first acentric high-pressure borate displaying edge-sharing BO_4 tetrahedra, Chem. Eur J. 26 (2020) 6851–6861, https://doi.org/10.1002/chem.201905419.

[50] M. Mutailipu, J. Han, Z. Li, F. Li, J. Li, F. Zhang, X. Long, Z. Yang, S. Pan, Achieving the full-wavelength phase-matching for efficient nonlinear optical frequency conversion in $C(NH_2)_3BF_4$, Nat. Photonics 17 (2023) 694–701, https://doi.org/10.1038/s41566-023-01228-7.

[51] C. Jin, H. Zeng, F. Zhang, H. Qiu, Z. Yang, M. Mutailipu, S. Pan, Guanidinium fluorooxoborates as efficient metal-free short-wavelength nonlinear optical crystals, Chem. Mater. 34 (2022) 440–450, https://doi.org/10.1021/acs.chemmater.1c03974.

[52] L. Jun, X. Shuping, G. Shiyang, FT-IR and Raman spectroscopic study of hydrated borates, Spectrochim. Acta, Part A 51 (1995) 519–532, https://doi.org/10.1016/0584-8539(94)00183-C.

[53] K. Nakamoto, M. Margoshes, R.E. Rundle, Stretching frequencies as a function of distances in hydrogen bonds, J. Am. Chem. Soc. (1955) 6480–6486.

[54] R. Kaindl, G. Sohr, H. Huppertz, Experimental determinations and quantum-chemical calculations of the vibrational spectra of β-ZnB_4O_7 and β-CaB_4O_7, Spectrochim. Acta, Part A 116 (2013) 408–417, https://doi.org/10.1016/j.saa.2013.07.072.

[55] J.P. Laperches, P. Tarte, Spectres d'absorption infrarouge de borates de terres rares, Spectrochim. Acta, Part A 22 (1966) 1201–1210.

[56] S.D. Ross, The vibrational spectra of some minerals containing tetrahedrally co-ordinated boron, Spectrochim. Acta (1972) 1555–1561.